Control of Self-Assembled Structures in Binary Mixtures of A−B Diblock Copolymer and A−C Diblock Copolymer by Changing the Interaction between B and C Block Chains†

Kohtaro Kimishima,‡,⊥ Hiroshi Jinnai,‡,# and Takeji Hashimoto*,‡,§

Hashimoto Polymer Phasing Project, ERATO, Japan Science and Technology Corporation, 15 Morimoto-cho, Shimogamo, Kyoto 606-0805, Japan, and Department of Polymer Chemistry, Graduate School of Engineering, Kyoto University, Kyoto 606-8501, Japan

Received December 4, 1998; Revised Manuscript Received February 16, 1999

ABSTRACT: Self-assembled structures in solvent-cast mixtures of polystyrene-*block*-poly(ethylenepropylene) (PS−PEP) and polystyrene-*block*-(partially hydrogenated polyisoprene) (PS−HPI) were investigated by small-angle X-ray scattering and transmission electron microscopy. Various self-assembled structures were observed in the solution-cast films, depending upon the degree of hydrogenation of the HPI block of the PS−HPI. The microdomain structure of PS domains and domains composed of PEP and HPI (called "rubber domains" hereafter) was first formed at relatively low polymer concentrations during the solvent-casting process over the whole range of the hydrogenation in our experiments. Subsequently, at a higher concentration during the process, phase separation between PEP and HPI in the rubber domains was observed in mixtures with medium and high hydrogenation. For mixtures with low hydrogenation, repulsive interactions between PEP and HPI become large enough to cause the segregation between PEP and HPI, which leads first to the modulation of the interface between the PS domain and the rubber domain and eventually to the macrophase separation between PS−PEP and PS−HPI, during the solvent evaporation process. Thus, observed macrophase-separated structure is a consequence of a two-step phase separation, i.e., a microphase separation followed by a macrophase separation. The development of those patterns was controlled only by the degree of the repulsive segmental interaction between PEP and HPI, i.e., the degree of the hydrogenation of HPI.

I. Introduction

Block copolymers consisting of different kinds of polymers chemically jointed together by a covalent bond form microdomain structures due to the segregation between the constituents. A variety of morphologies such as alternating lamellar, cylindrical, and spherical microdomains have been found according to the volume fraction of one of the constituents ("block composition").[1−3] Besides these "classical" morphologies, the bicontinuous structures, e.g., gyroid and perforated layers, were reported as new equilibrium structures of diblock copolymers.[4,5] Owing to the richness of the morphologies and their high regularity, control of the morphologies of block copolymers has been a current topic in polymer science and complex liquids (or soft-condensed matters).

Mixing a block copolymer with a homopolymer is a certain way to control the morphologies. The morphologies and the phase diagrams of the mixtures of an A−B block copolymer and an A homopolymer (denoted as A−B/A) were explored theoretically[6,7] and experimentally[8−15] in the past few decades. In those studies, it has been found that the way of the solubilizing A homopolymer in the A domains is an important factor in determining the morphologies. If the molecular weight of the A homopolymer is smaller than that of the A block chain (i.e., "wet brush" region[11−13,16]), the A homopolymers more or less uniformly dissolve in the A domains. This uniform solubilization in A domains effectively changes the volume occupied by each block chain and hence modifies the curvature of the interface, which then leads to the morphology change. On the other hand, if the molecular weight of the A homopolymer is larger than or about equal to that of the A block chain (i.e., "dry brush" region[11,13,16]), the A homopolymer tends to locate in the middle of the A domains. In such cases, the local curvature of the interface formed by block copolymer is hardly affected by homopolymers. The local structure of the domains is kept, and vesicle structures are generated.[13,16]

Adding chemically different polymers other than A and B to the two-component systems of A and B may extend the variation of the morphologies. There are two ways to do so: chemically linking C polymer to A−B diblock copolymer to make a triblock copolymer (A−B−C)[17−23] and mixing C homopolymer with A−B diblock copolymer (A−B/C).[24,25] The former system has only one kind of chain, while the latter has two different kinds of chains, although they both have three components. New microdomain structures were found in the A−B−C triblock copolymers such as the ordered tricontinuous double-diamond structure,[20,21] the microphase-separated structure in which middle block B formed a sphere at the interface between A and C lamellar domains,[22] and complicated morphology of A cylinder surrounded by B rings in a C matrix.[23] Thus, compared with the A−B diblock copolymers, the A−B−C triblock copolymers are very rich in morphologies. On the basis of conjecture about the A−B/A mixtures, the variation of

* To whom correspondence should be addressed.

† Presented in part at the American Chemical Society Meeting in Orlando, Aug 1996.

‡ Hashimoto Polymer Phasing Project, ERATO.

§ Department of Polymer Chemistry, Graduate School of Engineering, Kyoto University.

⊥ Present address: Tonen Chemical Corp., 3-1 Chidori-cho, Kawasaki, Kanagawa 210-0865, Japan.

Present address: Department of Polymer Science and Engineering, Kyoto Institute of Technology, Matsugasaki, Kyoto 606-8585, Japan.

10.1021/ma981892e CCC: $18.00
Published on Web 03/27/1999

morphologies in A−B/C would be even wider. One has to now consider the new items described below. Up to now, little attention has been given to the A−B/C systems.

One of the significant differences of A−B/A or A−B/C mixtures from the pure diblock copolymer is the existence of an interplay between two kinds of phase separations.[8] One is the macrophase separation that occurs between two constituent polymers, i.e., the block copolymer and the homopolymer (denoted hereafter as macrophase separation or transition). The other is the microphase separation of block copolymers themselves (denoted hereafter as microphase separation or transition). The coupling or interplay of these two kinds of phase separations (called as "complex phase transition or separation") gives rise to a rich variety of the self-assembled structures.[8] One example of the interplay of both macro- and microphase transitions is reported by Hashimoto et al.[24,25] They reported self-assembled patterns in a mixture of poly(oxy-2,6-dimethyl-1,4-phenylene) (PPO) and polystyrene-*block*-polyisoprene (SI) in a solvent-casting film.[24] The mixture showed unique patterns having two characteristic lengths, Λ_{macro} and Λ_{micro}. The microdomain structure having the size of Λ_{micro} ($\sim$100 nm) changes spatially with the long period Λ_{macro} ($\sim$5 μm) from a lamellar to sphere via a cylinder. In the PPO/SI system, concentration fluctuations of PPO and SI were first developed by the macrophase transition, in this case by the spinodal decomposition, which was followed by the microphase transition of SI. During the formation of microdomains of the SI diblock copolymer, PPO was selectively dissolved into the PS microdomains of the SI block copolymer and changed the effective volume fraction of the microdomains formed by PS and PI block chains. Since the spatial concentration of PPO was periodically changed, the morphology of the microdomain formed after the macrophase transition was also periodically varied in space.

Even in the case when only microphase separation occurs in the A−B/C mixture in some cases, there is still a difference in microdomain structures compared with those in A−B/A mixture. For example, in the mixture of poly(α-methylstyrene) (PαMS) and PS-*block*-PB-*block*-PS (SBS), a spatial distribution of PαMS homopolymer in the PS microdomains of SBS triblock copolymer was reported.[26] In this case the PαMS tended to localize in the middle of PS microdomains and made the distribution of the lamellar domain spacing somewhat broad, which are not usually observed in A−B/A systems. The origin of the localization of added homopolymer in the PS domain was the repulsive interaction between PαMS homopolymer and PS of the block copolymer. A balance of the interaction parameters, χ, among the three components had a significant role in controlling the morphology.

In the present paper, we are concerned with three-component binary mixtures of A−B and A−C diblock copolymers as an extension of the A−B/C system. Besides all of the complicated factors controlling the morphologies, the A−B/A−C system has unique points described below that are not present in A−B/C systems. If only microphase separation occurs, how do the two block copolymers self-assemble themselves in space? Three independent domains consisting of each component or two phases with one component separating from the other two would be interesting examples. If macrophase separation between A−B and A−C occurs, the structure of the macrodomains would be affected by the morphologies of the block copolymer. The focus of the A−B/C system was mainly whether and how the C homopolymer dissolves in one of the microphase-separated A or B domains. The variation of morphology of the A−B/A−C system would be even richer than the A−B/C system. Quite recently, Jeon et al. reported the self-assembled structures in binary blend of a polystyrene-*block*-polyisoprene and a polystyrene-*block*-poly(ethylenepropylene) diblock copolymer.[27] They reported a variety of morphologies as a function of blend composition, molecular weight of the block copolymer, and solvent evaporation rate and demonstrate an interplay of macrophase and microphase separations.

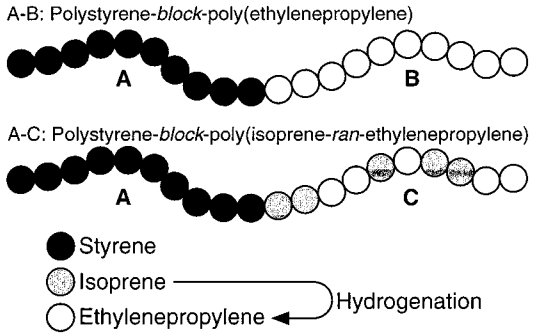

Figure 1. Schematic diagram of the block copolymers used in this study. White, gray, and black circles represent ethylenepropylene, isoprene, and styrene units, respectively. The isoprene units were modified to ethylenepropylene units by the hydrogenation reaction described in the text.

Although the A−B/A−C systems are interesting, many parameters such as the blend composition, the degree of polymerization, and the block compositions of each block and the segmental interaction parameters χ (χ_{AB}, χ_{AC}, χ_{BC}) have to be varied to make it clear how the morphology of the A−B/A−C system depends on these parameters. Here, in the present paper, we focus on investigating effects of the segmental interaction parameter between B and C block on the morphologies of the mixtures of A−B/A−C. For this purpose we introduced the random copolymer composed of B and D monomers to the block chains C; i.e., the A-*block*-B/A-*block*-(B-*ran*-D) system was used. In more detail, a block copolymer A-*block*-D was first synthesized and then modified to A-*block*-(B-*ran*-D) by a chemical modification of D repeating units, and by a complete modification, A-*block*-B was obtained. By controlling the degree of the reaction from D to B, the strength of the interaction between B chains of A-*block*-B and B-*ran*-D chains of A-*block*-(B-*ran*-D) was systematically changed, while keeping the total degree of polymerization of these two block copolymers unchanged.

II. Experimental Section

1. Samples. Figure 1 shows a schematic diagram of the sample used in this study. Polystyrene-*block*-poly(ethylenepropylene) (hereafter denoted as PS−PEP) and polystyrene-*block*-poly(isoprene-*ran*-ethylenepropylene) (denoted as PS−HPI) were used for A−B and A−C diblock copolymers, respectively. Both PS−PEP and PS−HPI were synthesized by hydrogenation of the same polystyrene-*block*-polyisoprene (PS−PI) having a number-average molecular weight (M_n) of 2.58×10^4 and a polydispersity index (M_w/M_n) of 1.14 with M_w being a weight-average molecular weight. The weight fraction of PS in PS−PI was 0.50. Perfect hydrogenation of PS−PI yielded PS−PEP

Table 1. Characteristics of the Samples Used in This Study

sample	material	M_w[a]	M_w/M_n[a]	w_{PS}[b]	ρ_{HPI}[c] (g/cm^3)	p[b,d] (mol %)
PS−HPI00	polystyrene-*block*-polyisoprene	2.58×10^4	1.14	0.500	0.900	0
PS−HPI20			1.14	0.499		17.9
PS−HPI30	polystyrene-*block*-		1.14	0.498		31.1
PS−HPI40	poly(isoprene-*ran*-		1.14	0.497		42.6
PS−HPI50	ethylenepropylene)		1.14	0.496		51.0
PS−HPI60			1.14	0.495		63.2
PS−PEP	polystyrene-*block*-poly(ethylenepropylene)		1.14	0.493	0.856	99.8

[a] Measured with GPC chromatography. [b] Determined by ^{1}H NMR spectroscopy. [c] Density of HPI block (ref 46). [d] Degree of hydrogenation of HPI block.

and partial hydrogenation, PS−HPI. The PI block in PS−PI had the microstructure of 94 mol % 1,4-linkage and 6 mol % 1,2-linkage, which was determined by ^{1}H NMR.

Hydrogenation was carried out using a reaction with diimide formed from the thermal decomposition of *p*-toluenesulfonylhydrazide (TSH).[28]

$$CH_3C_6H_4SO_2NHNH_2 \rightarrow CH_3C_6H_4SO_2H + HN{=}NH$$

$$R_2C{=}CR_2 + HN{=}NH \rightarrow R_2CH{-}CHR_2 + N_2$$

PS−PI and TSH were dissolved in toluene, and the reaction was carried out under a nitrogen atmosphere at 120 °C. The degree of the hydrogenation, p, was controlled by the reaction time. After the reaction, hydrogenated polymers were purified by the reprecipitation into methanol for a few times to remove the unreacted TSH. No gelation and no degradation were observed by gel permeation chromatography (GPC) measurement, and the random distribution of saturated ethylenepropylene units in the HPI block was confirmed by ozonolysis−GPC measurement.[29] The detailed effect of the hydrogenation on the physical properties of block copolymer will be described elsewhere.[30]

A series of PS−HPI having various p from 10 to 60 mol % were synthesized. Hereafter we denote p of PS−HPIs by a two-digit number in their abbreviated names. For example, the PS−HPI40 diblock copolymer had 40 mol % hydrogenation in the HPI block. The molecular characteristics of the polymers used in this study are summarized in Table 1.

PS−PEP and PS−HPI were mixed with 50 wt/50 wt composition and dissolved in toluene to be about 5 vol % of total polymer concentration. The solvent was allowed to evaporate in Petri dishes for 2 weeks at 30 °C. As-cast films thus obtained were further dried under vacuum at room temperature until no weight loss was observed. The ordered structure in the film was investigated by means of small-angle X-ray scattering (SAXS) and transmission electron microscopy (TEM).

2. TEM Observation. Small pieces of unstained films were embedded in an epoxy resin. The epoxy resin was hardened at 60 °C for 2 h. After trimming the specimen, it was microtomed to ultrathin sections of about 50 nm thickness using a Reichert Ultracut S with the cryochamber FCS operated at −110 °C. The sections thus obtained were exposed to osmium tetraoxide (OsO_4) vapor at room temperature for about an hour to stain selectively unsaturated isoprene units in HPI. In some cases, we further exposed the sections to ruthenium tetraoxide (RuO_4) to stain PS microdomains. Then the microdomain structures in the ultrathin sections were observed by a TEM (JEOL JEM-2000FXZ) operated at 160 kV.

3. SAXS Measurement. SAXS measurements were conducted with an apparatus consisting of an 18 kW rotating-anode X-ray generator (M18XHF-SRA, MAC Science Co. Ltd., Yokohama, Japan) with a graphite crystal monochromator, a three-slit collimator, a vacuum path for incident and scattered X-rays, and a one-dimensional position-sensitive proportional counter (PSPC). The sample-to-detector distance was about 2 m. A Cu Kα line beam with a wavelength of 0.1542 nm was used. The SAXS measurements were carried out under the condition where the line-collimated incident X-ray beam being parallel to the surface of the stacked film sample and the direction of the detector was perpendicular to the film surface (edge view). The SAXS profiles were corrected for the absorption of the sample, background scattering, and the thermal diffuse scattering arising form the acoustic phonons. Further correction for slit-smearing was performed when necessary.

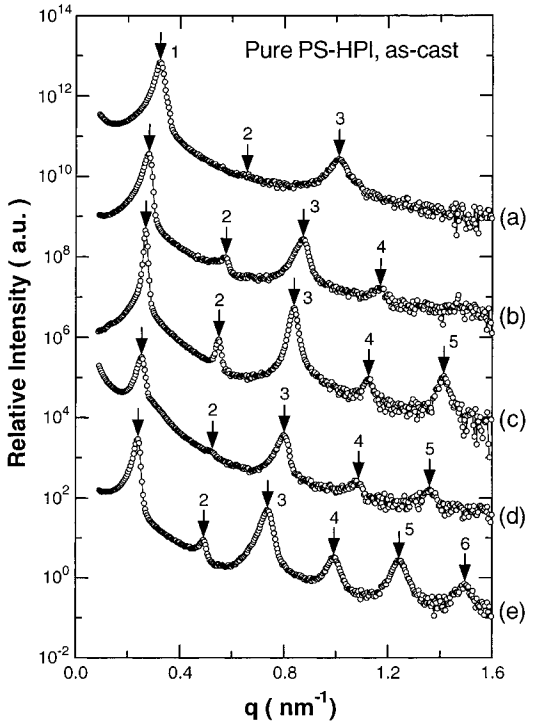

Figure 2. SAXS profiles for as-cast films of pure diblock copolymers having various degrees of the hydrogenation of (a) 0, (b) 31.1, (c) 42.6, (d) 63.2, and (e) 99.8 mol % taken at 27 °C. The first-order and higher-order scattering maxima shifted toward smaller q with increasing the degree of hydrogenation.

III. Results

1. Microdomain Structure of Pure Diblock Copolymers. Figure 2 shows the SAXS profiles taken at 27 °C for as-cast films of pure PS−HPI diblock copolymers having various p. The logarithm of the SAXS intensity is plotted against the magnitude of scattering vector, q, defined by $q = (4\pi/\lambda)\sin(\theta/2)$ with λ and θ being the wavelength of incident X-ray and the scattering angle, respectively.

All SAXS profiles showed higher-order scattering maxima at the positions of integer multiples relative to the position of first-order scattering maximum, indicating that alternating lamellar microdomains of PS and HPI were formed. The second- and forth-order peaks were very small compared with third- and fifth-order peaks. This means that the volume fraction of PS domains was approximately half for all samples. With increasing p (from profiles a−e) the peak position shifted toward smaller q, indicating the domain spacing, D, defined by

$$D = 2\pi/q_m \quad (1)$$

increased. Here q_m is magnitude of the scattering vector for the first-order scattering maximum. The domain spacing of lamellar microdomains of A−B diblock copolymer basically depends on the degree of polymerization, N, of the block copolymer and χ between A and B polymers, χ_{AB}. In our case the values N of PS−HPIs were same because they were prepared from the same PS−PI diblock copolymer. The increase in D indicates that χ_{AB} becomes large as p is increased. The long-range order of the microdomain structure is also increased as χ_{AB} (χ_{PS-HPI}) gets larger. Therefore, the higher the hydrogenation, the more the scattering maxima became visible.

Figure 3 shows the temperature dependence of the domain spacing of PS−HPI, D_{PS-HPI}, having various p plotted against absolute temperature, T, on a double-logarithmic scale. Data taken for T above 360 K were presented in order to avoid the nonequilibrium effect due to the glass transition of the PS microdomains. The measurement was carried out in the heating process. After measuring at the highest temperature, we remeasured the D value at 116.1 °C. The D value thus obtained was the same as that observed at 116.1 °C for the same sample before raising to the highest temperature, confirming effectively no sample degradation during the heating process. The solid line at the bottom of the figure shows the following relationship:

$$D \sim T^{-1/3} \quad (2)$$

which is fairly consistent with the experimental results on D_{PS-HPI} vs T at all hydrogenation levels. The same temperature dependence of D was previously reported for the PS−PI diblock copolymer.[31] The T and p dependence of D will be discussed to estimate χ parameters between the constituents in section IV.1.

2. Self-Assembled Structure in Blend Samples. *(a) TEM Observation.* Figure 4 shows the transmission electron micrographs of the binary mixtures of PS−PEP and PS−HPI00 (part a) and PS−HPI30 (parts b and c). In the TEM micrographs of (a) and (b), the staining was carried out using both OsO_4 and RuO_4 (denoted hereafter as "double staining"), while only OsO_4 was used in the TEM micrograph (c). Note that OsO_4 and RuO_4 stain respectively the HPI and PS domains.

In these mixtures two macroscopic domains ("macrodomains") were observed (see for example Figure 4c). Figure 4a shows the microdomain structure inside the respective macrodomains and the boundary between those macrodomains of the PS−PEP/PS−HPI00 mixture. In this figure two macrodomains were respectively composed of dark-and-gray lamellar microdomains (upper right side of the figure for the PS−HPI00 macrodomains) and bright-and-gray lamellar microdomains (lower left side for the PS−PEP macrodomains). Since the PEP domains were not stained with either OsO_4 or RuO_4, they appeared bright. The gray domains were PS domains selectively stained by RuO_4. The dark domains were PI domains stained by both OsO_4 and RuO_4. In the PS−HPI00 macrodomain in the upper right side of Figure 4a, the PS and HPI00 microdomains appeared gray and dark, respectively, while in the lower left side of Figure 4a, the PS and PEP microdomains appeared gray and bright, respectively. The lamellar spacing of PS−PEP microdomains was larger than that of PS−HPI00 microdomains, which is consistent with the SAXS results shown in Figure 2.

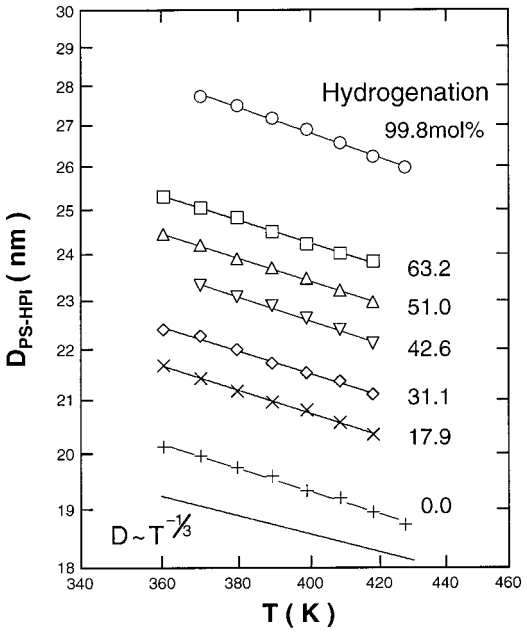

Figure 3. Temperature dependence of the domain spacing, D_{PS-HPI}, of PS−HPI having various degrees of hydrogenation. The solid line shows the power law of $D \sim T^{-1/3}$.

Figure 4b shows the TEM micrograph of the PS−PEP/PS−HPI30 mixture. The macrodomains of PS−PEP and PS−HPI were also observed; the bright and gray lamellae respectively correspond to the PEP and PS lamellae in the PS−PEP macrodomains (marked A), while the gray and dark lamellae respectively correspond to the PS and PI lamellae in the PS−HPI30 macrodomains (marked B). The size of the macrodomains, however, was small compared with those of the PS−PEP/PS−HPI00 mixture. This may reflect that the net repulsive interaction between two block copolymers decreased with increasing p. Figure 4c taken with a lower magnification than in Figure 4b highlights spatial distributions of the macrodomains. PS−HPI30 macrodomains appeared dark, because HPI30 was stained with OsO_4, and PS−PEP macrodomains appeared bright, because both PS and PEP were not stained with OsO_4. It is worth noting that the shape of macrodomains is somewhat elongated. The interface between the two macrodomains are not smooth and round (see Figure 4c). The origin of these observations will be discussed in section IV.5.

Figure 5 shows TEM micrographs of binary mixtures of PS−PEP and PS−HPI having 40 mol % (parts a and b) and 60 mol % (parts c and d) hydrogenation. In these mixtures only microphase separation but no macrophase separation was observed. The insets in Figure 5a,c are schematic illustrations of the microdomain structures of these mixtures. Two ultrathin sections cut from the same films embedded in the epoxy resin were prepared; one of them was stained only with OsO_4 (top parts a and c), and the other was subjected to the double staining (parts b and d). The alternating lamellar microdomains appearing bright and dark were observed for OsO_4 staining sample (parts a and c). It is worth pointing out that the bright areas can be observed inside the dark microdomains in both parts a and c of Figure 5. Since the dark areas are HPI regions where the unsaturated double bonds were stained with OsO_4, the

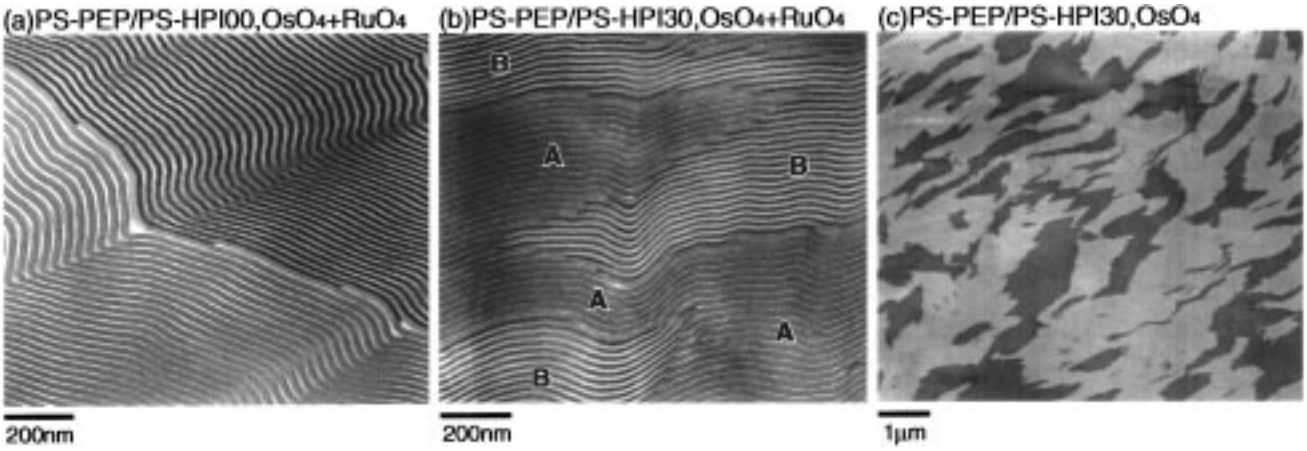

Figure 4. TEM micrographs of the PS−PEP/PS−HPI00 mixture (part a) and the PS−PEP/PS−HPI30 mixture (parts b and c) taken at different magnifications. The macrophase-separated structure between PS−PEP and PS−HPI was observed in both mixtures.

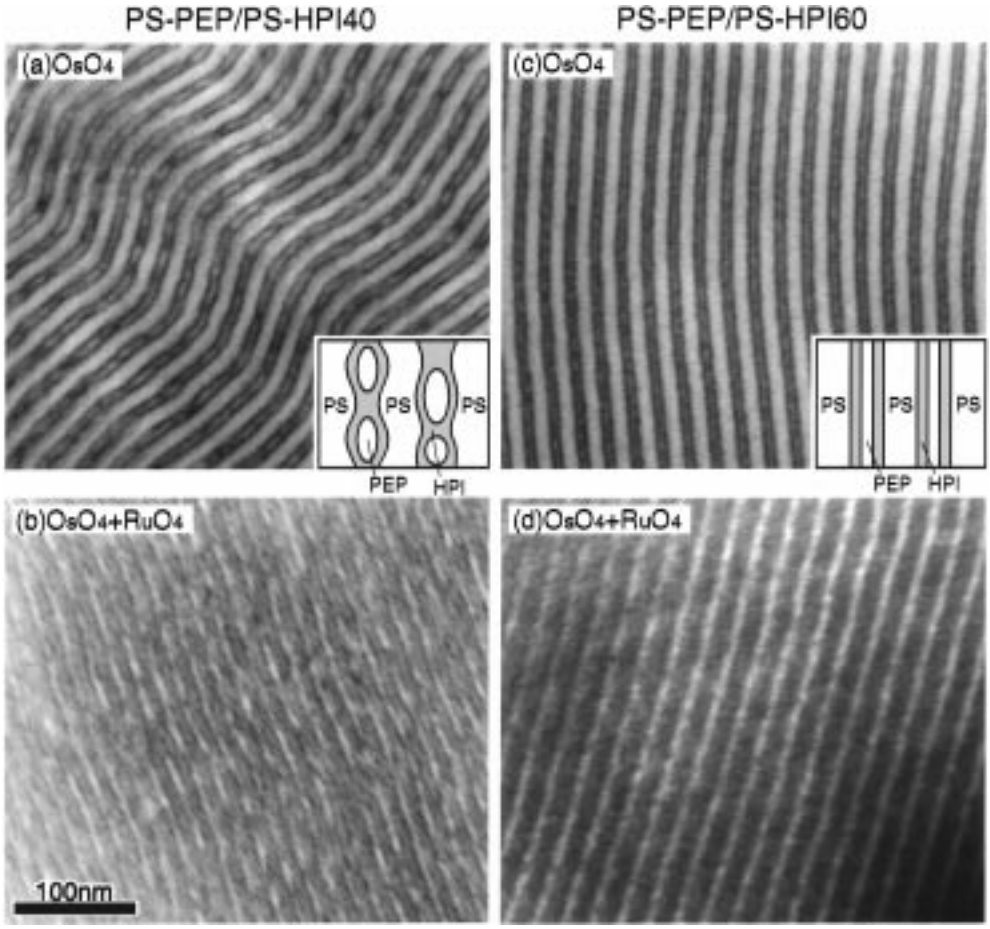

Figure 5. TEM micrographs of the PS−PEP/PS−HPI40 mixture (parts a and b) and the PS−PEP/PS−HPI60 mixture (parts c and d). The top two micrographs (a and c) were obtained with the thin sections stained with OsO_4, and the bottom two micrographs were obtained with the thin sections stained with OsO_4 and RuO_4. The inset pictures in parts a and c are the schematic diagram of the observed microdomain structures.

bright areas inside the HPI domains are PEP domains. Note that PS domains also are not stained with OsO_4, which appeared as thick bright lamellae.

The PEP microdomains were mostly discontinuous along the lamellar interface in the PS−PEP/PS−HPI40 mixture, while in the PS−PEP/PS−HPI60 mixture they were uniformly distributed along the interface. This difference in the distribution of PEP domains was clearly demonstrated in the double-stained samples (parts b and d), in which only the PEP microdomains are left unstained and appear bright, while PS and HPI domains appear dark. The discontinuity of the PEP domains was obvious in the PS−PEP/PS−HPI40 mixture. Thus, the microdomain structures shown here should be considered as the microdomains of PS lamellae and the lamellae composed of PEP and HPI (hereafter denoted as "rubber domains"). In the rubber domains of the PS−PEP/PS−HPI40 mixture, the PEP microdomains are discontinuous in the HPI matrix, generating a unique three-phase coexistence as il-

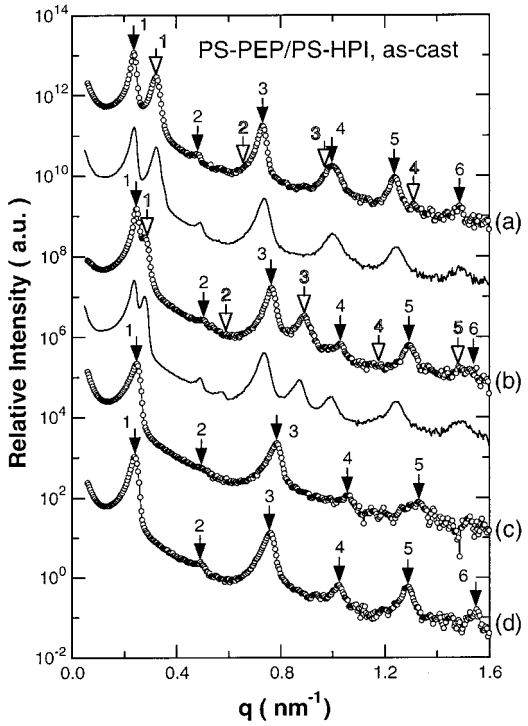

Figure 6. SAXS profiles of as-cast films of the binary mixtures of PS−PEP and (a) PS−HPI00, (b) PS−HPI30, (c) PS−HPI40, and (d) PS−HPI60, measured at 27 °C. Solid lines below the profiles a and b are the volume-averaged SAXS profiles of the neat block copolymers comprising the mixtures.

lustrated in the inset of part a, while they are continuous and sandwiched with the HPI lamellae, generating the three-phase coexistence composed of PS, HPI, PEP, and HPI lamellae as a repeating unit (inset of part c) in the PS−PEP/PS−HPI60 mixture.

(b) SAXS Measurements. Figure 6 shows the SAXS profiles of as-cast films of PS−PEP/PS−HPI mixtures. SAXS profiles a, b, c, and d were obtained from the mixtures of PS−PEP and PS−HPI00, PS−HPI30, PS−HPI40, and PS−HPI60, respectively. First, we describe the SAXS profiles (a and b) from the mixtures that showed macrodomains (see parts a and b of Figure 4 for TEM micrographs, respectively). Solid line under the plots a and b are calculated SAXS profiles, $I_{calc}(q)$, based on the following equation:

$$I_{calc}(q) = \phi_{PS-PEP} I_{PS-PEP}(q) + (1 - \phi_{PS-PEP}) I_{PS-HPI}(q) \quad (3)$$

where ϕ_{PS-PEP} is the volume fraction of PS−PEP in the mixtures. The curves $I_{PS-PEP}(q)$ and $I_{PS-HPI}(q)$ are the SAXS profiles of constituent neat diblock copolymers ($I_{PS-HPI}(q)$: profile a for PS−HPI00 and profile b for PS−HPI30 in Figure 2; $I_{PS-PEP}(q)$: profile e in Figure 2). The calculated profiles obtained for $\phi_{PS-PEP} = 0.507$ were found to be in very good agreement with measured profiles in terms of the peak position as well as the relative peak height of higher-ordered peaks. This indicates that the constituent block copolymers were almost perfectly phase-separated, and the microdomains in each macrodomains were made of the nearly pure diblock copolymer. The black and white arrows labeled with integer numbers in Figure 6 show that the peaks can be assigned to the PS−PEP and PS−HPI lamellar microdomains, respectively.

Second, let us describe the mixtures showing only microdomain structures, i.e., PS−PEP/PS−HPI40 (profile c) and PS−PEP/PS−HPI60 (profile d). It was found that the scattering profile from the uniform lamellar microdomains (profile d) is similar to those for neat two-component block copolymers;[32] that is, the peak positions of higher-order scattering maxima were integer multiples of q_m. The domain spacing D for those mixtures obtained from eq 1 were between those of pure PS−PEP and PS−HPI, indicating that the effective repulsive interaction between the two lamellar microdomains in those mixtures (PS domains and the rubber domains as shown in TEM of Figure 5) was between that of PS and PEP and that of PS and HPI (HPI00 or HPI30). The scattering profile for PS−PEP/PS−HPI40 (profile c) also exhibits that characteristic of (pseudo) two-component lamellar microdomains, though the long-range order of the microdomains is somewhat less compared with that of PS−PEP/PS−HPI60 (profile d), judging from the weaker intensity of higher-order peaks. This means the lamellar microdomains is somewhat distorted, which is in agreement with TEM results.

IV. Discussion

1. Estimation of Interaction Parameters. Since it is a competition of the microphase and the macrophase transitions that determines the phase-separated structures in the PS−PEP/PS−HPI systems, it is essential to estimate the three interaction parameters between the constituent polymers, from which the stability limits of the two kinds of phase separations for the A−B/A−C system can be calculated. Direct determination of the interaction parameters involves analyses of scattering functions in the disordered state of the A−B (or A−C) block copolymer.[33] However, some block copolymers used in the present study, e.g., PS−PEP, never exhibit the disordered state within the accessible temperature range, i.e., from room temperature to ca. 200 °C. Therefore, in this section, we try to estimate the interaction parameters from the domain spacing of the microphase-separated structures of the pure diblock copolymers.

The domain spacing of the lamellar microdomains of a diblock copolymer, D, is given by[31]

$$D \propto \chi^{1/3} N^{2/3} \quad (4)$$

where χ is the Flory's segmental interaction parameter between the constituents such as between PS and PI, and N is the degree of polymerization of the block copolymer. Since PS−HPI and PS−PEP block copolymers used here were made by hydrogenation of the same PS−PI diblock copolymer to different extents, N is essentially the same for all diblock copolymers. Strictly speaking, D also depends on the density of the polymer. The density of PEP is smaller than that of PI (see Table 1), which could lead the domain spacing of PS−PEP, D_{PS-PEP}, to be a little larger than that of PS−PI, D_{PS-PI}. Note that PI is an extreme case of hydrogenated polyisoprene, i.e., zero hydrogenation. Taking the density difference into account, the ratio of D_{PS-PEP} to D_{PS-PI} would be 1.028, while the measured ratio was $D_{PS-PEP}/D_{PS-PI} = 1.38$. This value was considerably larger than that estimated only from the density difference. Therefore, it is reasonable to assume that D depends primarily on χ. Since χ is related to the absolute temperature, T, through the following relationship:

$$\chi \propto 1/T \quad (5)$$

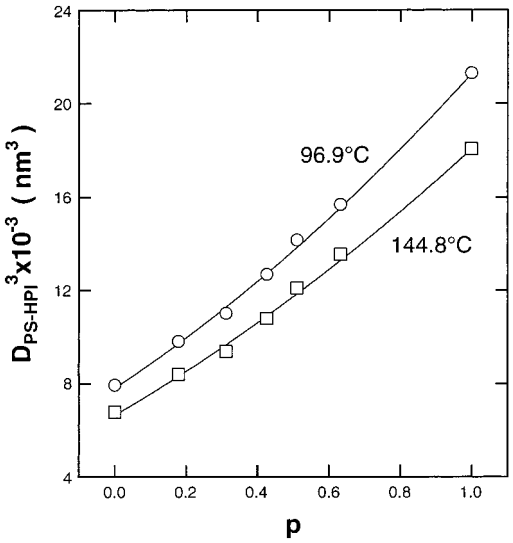

Figure 7. Plot of D_{PS-HPI}^3 vs p, based on eq 7 in text, at 96.9 °C (plotted by circles) and 144.8 °C (plotted by squares). The solid lines in the figure were the best-fitted curves with the quadratic form of p (eq 7).

D has a temperature dependence that can be predicted by eqs 4 and 5, as shown in Figure 3.

As mentioned earlier, the HPI blocks of PS−HPI are randomly hydrogenated; hence, the random copolymer theory[34,35] can be applied to the system. Thus, the effective interaction parameter between PS and HPI, χ_{PS-HPI}, can be written using the "fundamental" segmental interaction parameters such as χ_{S-EP}, χ_{S-I}, and χ_{EP-I} in the following way:

$$\chi_{PS-HPI} = p\chi_{S-EP} + (1-p)\chi_{S-I} - p(1-p)\chi_{EP-I} \quad (6)$$

Here χ_{i-j} represents the interaction parameter between i and j units with S, I, and EP being styrene, isoprene, and ethylenepropylene repeating units, respectively. Combining eqs 4−6, we obtain

$$D^3 \sim ap^2 + bp + c \quad (7)$$

with

$$a = k\chi_{EP-I} \quad (8)$$

$$b = k(\chi_{S-EP} - \chi_{S-I} - \chi_{EP-I}) \quad (9)$$

$$c = k\chi_{S-I} \quad (10)$$

where k is a proportional constant. From eqs 8−10, relative interaction parameters with respect to χ_{S-I} can be obtained as

$$\chi_{S-EP}/\chi_{S-I} = (a+b+c)/c \quad (11)$$

$$\chi_{EP-I}/\chi_{S-I} = a/c \quad (12)$$

On the basis of eq 7, D^3 at 96.9 and 144.8 °C are plotted against p in Figure 7. The solid lines in the figure show the best-fit quadratic curves (see eq 7). The relative interaction parameters with respect to χ_{S-I}, i.e., the quantities on the left-hand side of eqs 11 and 12, were determined from the parameters a, b, and c obtained from the fitting. The interaction parameters thus obtained are listed in Table 2, which showed little dependence on the temperature. The χ values at the solvent casting-temperature (30 °C) by linear extrapolation were

Table 2. Relative Interaction Parameters Evaluated from the Domain Spacings of Neat PS−HPI Diblock Copolymers Having Various Degree of Hydrogenation

T (°C)	χ_{S-EP}/χ_{S-I}	χ_{I-EP}/χ_{S-I}	T (°C)	χ_{S-EP}/χ_{S-I}	χ_{I-EP}/χ_{S-I}
96.9	2.71	0.429	125.7	2.72	0.449
106.5	2.74	0.475	135.3	2.68	0.418
116.1	2.72	0.462	144.8	2.70	0.372

$$\chi_{S-EP}/\chi_{S-I} = 2.79 \quad (13)$$

$$\chi_{EP-I}/\chi_{S-I} = 0.59 \quad (14)$$

These values will be used to estimate the stability limit of the PS−PEP/PS−HPI systems later in section IV.2.

From eqs 6, 13, and 14, the effective interaction parameter between PS and HPI with respect to χ_{S-I} can be written as

$$\frac{\chi_{PS-HPI}}{\chi_{S-I}} = p\frac{\chi_{S-EP}}{\chi_{S-I}} + (1-p) - p(1-p)\frac{\chi_{EP-I}}{\chi_{S-I}} = 0.59p^2 + 1.2p + 1 \quad (15)$$

which is a monotonically increasing function of p over the whole range, i.e., $0 \le p \le 1$. Thus, the following relationship is obtained:

$$\chi_{S-EP} > \chi_{PS-HPI} > \chi_{S-I} > \chi_{EP-I} > \chi_{PEP-HPI} \quad (16)$$

Here $\chi_{PEP-HPI}$ is the effective interaction parameter between PEP and HPI. The reason for the inequality $\chi_{EP-I} > \chi_{PEP-HPI}$ in eq 16 is because the following relation is realized if the random copolymer theory is applied under the assumption that HPI is a random copolymer of isoprene and ethylenepropyrene monomers:

$$\chi_{PEP-HPI} = p\chi_{EP-EP} + (1-p)\chi_{EP-I} - p(1-p)\chi_{EP-I} = (1-p)^2\chi_{EP-I} \quad (17)$$

2. Stability Limits for Macrophase and Microphase Transitions. The RPA theory[36] generalized for block copolymers was presented by Leibler, which gives the detailed formula of the scattering functions of A−B block copolymer[37] and the mixture of A−B block copolymer and A homopolymer[38,39] in the disordered state. Later the RPA theory was extended to three- or multicomponent polymer systems.[40,41] Ijichi et al.[40] presented a series of scattering functions in the disordered state, $I_{dis}(q)$, for various three-component systems including the binary mixtures of block copolymers A−B and A−C. The general formula of $I_{dis}(q)$ for the three-component system is given by

$$I_{dis}(q) \propto S(q;\chi_{A-B},\chi_{A-C},\chi_{B-C})/F(q;\chi_{A-B},\chi_{A-C},\chi_{B-C}) \quad (18)$$

where χ_{i-j} is the interaction parameter between i and j components. In our case A, B, and C correspond to PS, PEP, and HPI, respectively. The functions $S(q)$ and $F(q)$ contain the parameters which describe the characteristics of the system such as degree of polymerization, block composition, and blend ratio of A−B and A−C. The detailed formula of these functions is presented in ref 40. The stability limits for the macrophase and the microphase transitions are able to be computed by solving the following equations:

$$F(q = 0; \chi_{A-B}, \chi_{A-C}, \chi_{B-C}) = 0 \quad \text{(for macrophase transition)} \quad (19)$$

$$F(q \neq 0; \chi_{A-B}, \chi_{A-C}, \chi_{B-C}) = 0 \quad \text{(for microphase transition)} \quad (20)$$

For a given p and χ_{S-EP}, the other two interaction parameters, i.e., χ_{PS-HPI} and $\chi_{PEP-HPI}$, can be calculated from eqs 6, 13, 14, and 17, which were then used to calculate $F(q)$. The stability limit for the microphase and microphase transitions can be found respectively by finding χ_{S-EP} values satisfying eqs 19 and 20. ($\chi_{S-EP}N$) at the macrophase and the microphase stability limits thus obtained are plotted against p for the PS−PEP/PS−HPI (50 wt/50 wt) mixture in Figure 8 by the solid and the broken lines, respectively.

One of the extreme cases, i.e., $p = 1$, corresponds to the pure diblock copolymer (PS−PEP). In such a case, only microphase separation can occur, and the stability limit is $\chi_{S-EP}N = 10.495$, which is consistent with the theoretical value.[37] The other extreme case, $p = 0$, corresponds to the mixture of PS−PEP and PS−PI. In this case, it is possible that both macrophase and microphase transitions occur. The stability limit for the microphase transition becomes larger than that of pure PS−PEP because the repulsive interaction between PS and PI is lower than that between PS and PEP. On the other hand, the stability limit of the macrophase transition gets smaller with decreasing p due to the increase of the repulsive interaction between PEP and HPI.

The results shown in Figure 8 give a significant insight underlying the self-assembling process of our mixtures encountered in the solvent evaporation process. As solvent evaporates, the effective interactions χ_{ij} among the constituent block chains in the solution increase. This gives rise to an increase of the effective ($\chi_{S-EP}N$) value, eventually causing the microphase and macrophase separation. The results in Figure 8 predict that the microphase separation occurs prior to the macrophase separation for all the mixtures of PS−PEP/PS−HPI with 50 wt/50 wt composition studied in this work. This prediction will be tested in the next section.

3. SAXS from the PS−PEP/PS−HPI00 Mixture in Solution. In the previous sections, three interaction parameters between the constituent polymers were estimated, which were used for the numerical analysis of the stability limits of the PS−PEP/PS−HPI system as discussed above. The purpose of analyzing the stability limits is to understand how the various phase-separated structures shown in Figures 4 and 5 were formed. In the present section, we would like to simulate experimentally the casting process from toluene solution by examining the phase-separated structures at various concentrations. The toluene solution of PS−PEP/PS−HPI00 (50 wt/50 wt) mixture was chosen, because the macrophase separation may most likely occur in this system, as clarified in Figure 8.

A series of the mixtures having various total polymer concentrations, ϕ_p, from 12.3 to 60 vol % were prepared. The toluene solution having $\phi_p \geq 42$ vol % was turbid, demonstrating that the macrophase separation took place. Note toluene is a neutral solvent for PS and HPI00 (i.e., PI), while the neutrality for PEP is not known. However, since PEP dissolves in toluene at any concentration, the macrophase separation observed here occurred between PS−PEP solution and PS−HPI00 solution, not between the polymer and toluene. The solution was transparent if $\phi_p \leq 37.2$ vol %. Figure 9 shows the desmeared SAXS profiles of solutions with various ϕ_p taken at 27 °C on a double-logarithmic scale.

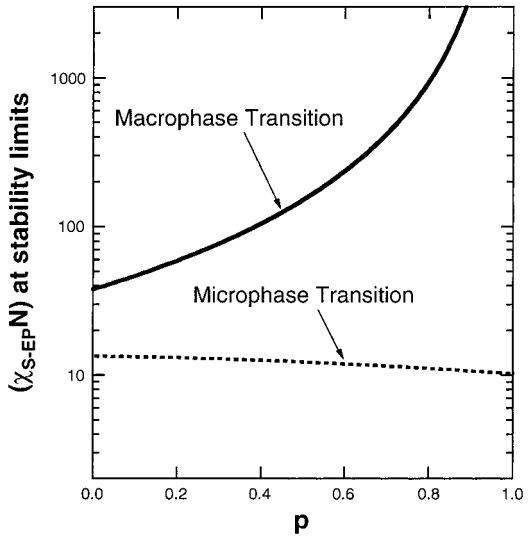

Figure 8. Spinodal curves for macrophase transition (solid line) and microphase transition (dashed line) for PS−PEP/PS−HPI (50 wt/50 wt) mixtures having various degrees of hydrogenation, p, in the HPI block, indicating the microphase transition is more unstable than macrophase transition for all mixtures.

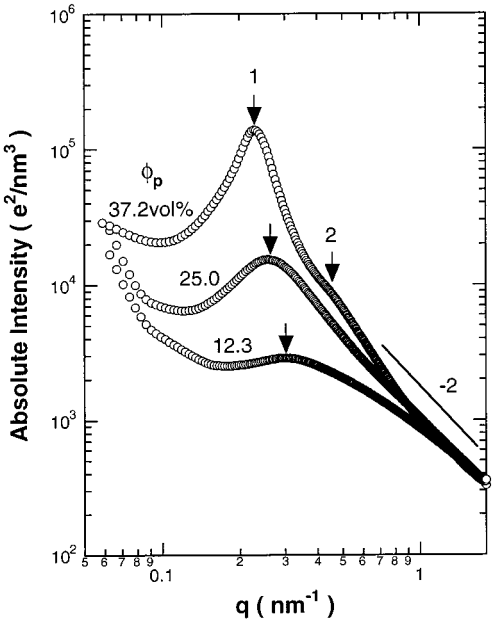

Figure 9. Desmeared SAXS profiles of the PS−PEP/PS−HPI00 (50 wt/50 wt) mixture in toluene solution having various total polymer concentrations.

At low ϕ_p (12.3 vol %) the SAXS profile showed a single broad peak, and the scattering intensity profile obeys q^{-2} in the high-q region of the figure. This indicates that the block copolymer mixture was in the disordered state. As the ϕ_p became larger, the peak intensity increased and the peak got sharper. At $\phi_p = 37.2$ vol % the shoulder at the position of 2 relative to q_m was discernible. Although the PS−PEP/PS−HPI00 eventually exhibited macrophase separation after the solvent casting (see Figure 4a) and the SAXS profile of the as-cast film clearly showed the higher-order peaks due to the phase-separated grains of lamellae having

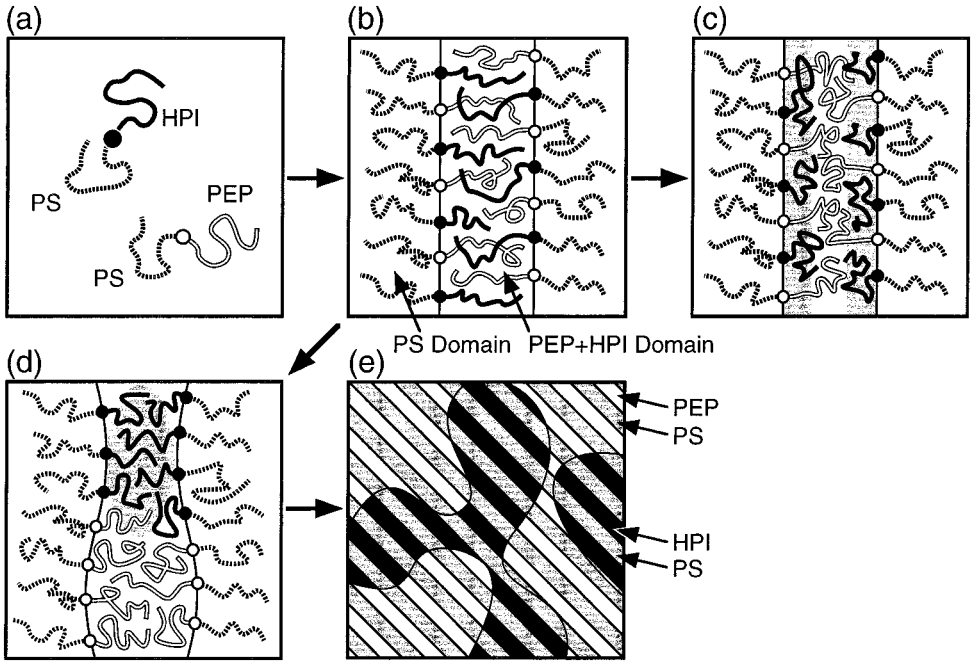

Figure 10. Schematic diagram showing the formation of self-assembled structures in PS−PEP and PS−HPI mixtures during the solvent evaporation process.

two different domain spacings (see Figure 6a), the mixture at $\phi_p = 37.2$ vol % had a single first-order and weak second-order scattering peak. This indicated that, at $\phi_p = 37.2$ vol % and thus in the initial stage of the solution casting, only microphase separation occurred. In other words, the microphase transition occurred from the disordered state earlier than the macrophase transition did, which is consistent with the phase diagram shown in Figure 8.

4. Processes of Self-Assembled Patterns. Figure 10 schematically shows a possible mechanism of the self-assembling processes in the PS−PEP/PS−HPI system. In the initial state of casting with toluene as a solvent, both PS−PEP and PS−HPI are dissolved in toluene in a single-phase and in a disordered state (Figure 10a). For simplicity, toluene is not drawn in the figure and assumed to be more or less uniformly distributed in space, forming a continuous medium. First, let us consider the phase separation process of mixture of PS−PEP and PS−HPI with relatively high hydrogenation such as 60%. As the toluene evaporates, the polymer concentration gets higher, and the microphase separation between the PS and "rubber" domains that consists of PEP and HPI first takes place (Figure 10b). Let us point out here that the system first becomes unstable for the microphase transition rather than the macrophase transition over the whole range of hydrogenation (see Figure 8). As the solvent further evaporates, the PS domain is vitrified due to the glass transition at some polymer concentration, c_g. For the PS−PI diblock copolymer in toluene solution, 70−75 vol % was reported for c_g.[42] In the case of the PS−PEP/PS−HPI60 system, the HPI60 chains are highly hydrogenated and thus miscible with PEP even at c_g. Upon further evaporating the solvent after the vitrification of the PS domain, PEP and HPI started to phase-separate inside the rubber domain, due to increased segregation power between PEP and HPI blocks at higher polymer concentration. However, since the junction points of block copolymers at the interface are fixed, diffusion of those molecules along the lamella interface is prohibited. Then phase separation inside the rubber domain takes place only in the direction perpendicular to the lamellar interface, which leads to the three components to distribute uniformly along the interface (Figure 10c).

As shown in SAXS profiles of pure diblock copolymers in Figure 2, PEP segregated from PS more strongly than HPI. Therefore, PEP chains tend to localize at the center of the rubber domains in order to avoid contact with PS. This localization, in turn, increases the loss of the conformational entropy of the PEP and HPI chains. Roughly speaking, the balance of these two thermodynamic factors (the energetic interactions of PS with PEP and HPI and the conformational entropies of HPI and PEP) may determine the degree of the localization of PEP.

Second, in the case of PS−PEP/PS−HPI40, microphase separation between the PS and rubber domains occurs just in the same way as the PS−PEP/PS−HPI60 system during the casting process. Since the hydrogenation is lower for the PS−HPI40 than for the PS−HPI60 and thus the repulsive interaction between HPI40 and PEP is larger than that between HPI60 and PEP, they may tend to segregate before the polymer concentration reaches c_g. If so, PEP and HPI40 chains start to undergo phase separation in the direction both parallel and perpendicular to the lamellar interface between the PS and the rubber domains in order to minimize the contact of each other (so that system changes from Figure 10b to Figure 10d). We would like to note that the domain spacing of pure PS−PEP is larger than that of pure PS−HPI40 by a factor of 1.2, which may lead the lamella interface to be somewhat undulated. Soon after the phase separation inside the rubber phase, the PS domain is vitrified as the polymer concentration exceeds c_g, which fixes the structure.

Macrophase separation occurred for both PS−PEP/PS−HPI30 and PS−PEP/PS−HPI00. In these mixture, since the HPI chains have a low p, the segregation power between PEP and HPI chains are stronger than the other mixtures. They therefore tend to segregate even earlier or at a lower polymer concentration than

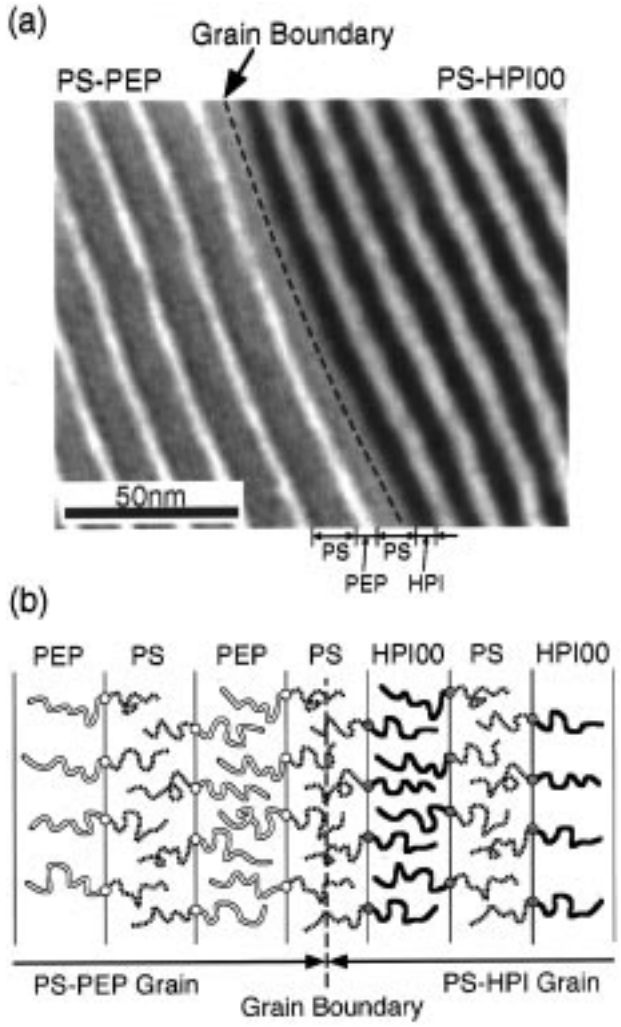

Figure 11. Typical TEM micrograph showing the grain boundary between PS−PEP and PS−HPI00 macrodomains stained with OsO_4 and RuO_4 (part a), showing the unique interconnection of PS, PEP, and HPI00 lamellae at the boundary without involving unfavorable segmental interactions as illustrated in the schematic diagram (part b).

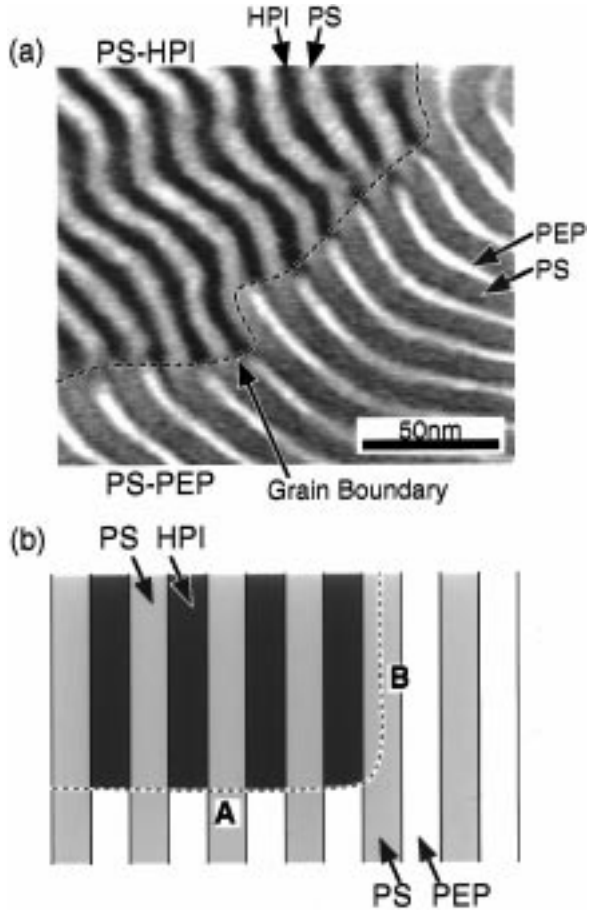

Figure 12. TEM micrograph showing the grain boundary between PS−PEP and PS−HPI00 macrodomains stained with OsO_4 and RuO_4 (part a). At the grain boundary of type A, HPI lamellae are connected to PEP lamellae, as shown in the schematic diagram b, which may cause higher free energy to the grain boundary of type B.

PS−PEP/PS−HPI40. The mixture follows exactly the same self-assembling process as the PS−PEP/PS−HPI40 mixtures, i.e., following the path form part a to part b and then to part d; however, even at the stage of Figure 10d, the polymer concentration would be below c_g, so that both PS−PEP and PS−HPI were movable. The modulated interface may cause higher interfacial energy in the system, which makes the microdomains such as Figure 10d unstable. This then causes the macrophase separation between PS−PEP and PS−HPI (the change from part d to part e in Figure 10). The block copolymers undergo translational diffusion either along the interface, keeping their chemical junctions on the interface, or across the interface. The diffusion along the interface may be faster than that through microdomains.[43,44] The diffusion of block copolymers across the interface may be increasingly restricted as the segregation power becomes large. This is because as the segregation power increases, the chemical junctions of the block copolymer became strongly localized at the interface. The glass transition of the PS domains also vitrifies the pattern growth (Figure 10e) upon further evaporation of the solvent. Thus, the degree of the interaction between PEP and HPI has a significant role in controlling the self-assembling process in the PS−PEP/PS−HPI mixtures, and the macrophase-separated structure is revealed to occur as a consequence of a two-step phase separation, i.e., the microphase separation followed by the macrophase separation. For the PS−PEP/PS−HPI00 mixture, the segregation power between the two block copolymers is stronger than that for the PS−PEP/PS−HPI30, so that their macrodomains grew bigger than those for the PS−PEP/PS−HPI30 before the vitrification at c_g.

5. Grain-Boundary Structures at Macrodomains. As shown in Figure 4c, the macrodomains composed of PS−PEP and PS−HPI which may have developed through the process explained in Figure 10 have an irregularity in shape; i.e., the grain boundary between the PS−HPI and PS−PEP grains was not smooth and round, which is substantially different from those of the phase-separated structure developed via spinodal decomposition in a binary viscous polymer mixture, in which the interface between two phases are smooth and round, and the domain structures show spongelike structures.[45] Figure 11 gives the magnified TEM micrographs at the grain boundary in the PS−PEP/PS−HPI00 mixture with double staining. Note that bright, gray, and dark lamella respectively are PEP, PS, and HPI00 microdomains. In this case the PS lamella lays at the grain boundary between the macrodomains of both PS−PEP (left side) and PS−HPI (right side) block

copolymer without paying an excess energy cost at the grain boundary. The schematic of chain packing is illustrated in part b of the figure. Both PS−PEP and PS−HPI lamellae in each macrodomain were aligned parallel to the grain boundary.

Figure 12 shows another TEM (part a) having a grain boundary different from that shown in Figure 11 and its corresponding sketch (part b). The image was again obtained on the double-stained ultrathin sections so that the interpretation of the bright, gray, and dark phases is same as that in Figure 11. In part b, the grain boundary marked B is the one discussed in Figure 11, but the grain boundary marked A is the one different from B. In this case the grain boundary is not parallel to the lamellar microdomains as in the grain boundary marked B but rather intersect with them. The PS lamellae from PS−PEP are connected to the PS lamellae from PS−HPI, and the PEP lamellae of PS−PEP are connected to the HPI lamellae from PS−HPI. The grain boundary of type A may have a higher free energy than that of type B, which may explain the anisotropic shape of the grains elongated along the direction parallel to the lamellar interface. The grains have irregular interfaces due to the elastic nature of lamellar microdomains comprising the grains.

V. Concluding Remarks

We have presented the self-assembled patterns for the mixture of PS−PEP and PS−HPI diblock copolymers developed during solvent casting. From the RPA calculation and the SAXS measurements of the samples as a function of polymer concentration, all structures shown in Figures 4 and 5 were found to be formed generally through a two-step phase separation process encountered in the solvent evaporation process: the microphase separation occurs first, developing the microdomain structure of the PS domains and the rubber domains composed of PEP and HPI. The degree of the repulsive interaction between PEP and HPI, which we were able to control by the degree of the hydrogenation of HPI, had a significant role in determining the second-step macrophase separation and hence the final structures. The large interaction causes the phase separation between PEP and HPI inside the rubber domains to develop the unique three-phase coexistence structure of lamellae as shown in Figure 5c,d and schematically illustrated in Figure 10c, the modulated interface of the microdomain as shown in Figure 5a,b and schematically in Figure 10d, or the macrophase-separated structure between PS−PEP and PS−HPI as shown in Figure 4 and schematically in Figure 10e. These macrodomains have an irregular shape and does not have smooth interface as found in phase-separating viscous binary systems, which is due to an elastic effect of lamellar microdomains comprising the phase-separating macrodomains and to a special interfacial free energy associated with a spatial connectivity of each lamellar microdomain at the macrointerfaces.

Acknowledgment. We are grateful to Dr. Tsuyoshi Koga for useful discussions. We thank Drs. K. Tsutsumi and Y. Hirokawa for helpful suggestions on the hydrogenation of the samples.

References and Notes

(1) Hashimoto, T.; Shibayama, M.; Fujimura, M.; Kawai, H. In *Block Copolymers, Science and Technology*; Meier, D. J., Ed.; Harwood Academic Publishers: London, 1983; pp 63−108. Hashimoto, T. In *Thermoplastic Elastomers*, 2nd ed.; Holden, G., Legge, N. R., Quirk, R., Schroeder, H. E., Eds.; Hanser: Munich, 1996; pp 429−494.

(2) Thomas, E. L.; Alward, D. B.; Kinning, D. J.; Martin, D. C.; Handlin, D. J., Jr.; Fetters, L. J. *Macromolecules* **1986**, *19*, 2197.

(3) Bates, F. S.; Fredrickson, G. H. *Annu. Rev. Chem.* **1990**, *41*, 525.

(4) Hajduk, D. A.; Harper, P. E.; Gruner, S. M.; Honeker, C. C.; Thomas, E. L.; Fetters, L. J. *Macromolecules* **1994**, *27*, 4063.

(5) Khandpur, A. K.; Förster, S.; Bates, F. S.; Hamley, I. W.; Ryan, A. J.; Bras, W.; Almdal, K.; Mortensen, K. *Macromolecules* **1995**, *28*, 8796.

(6) Hong, K. M.; Noolandi, J. *Macromolecules* **1983**, *16*, 1083.

(7) Whitmore, M. D.; Noolandi, J. *Macromolecules* **1985**, *18*, 2486.

(8) Hashimoto, T.; Tanaka, H.; Hasegawa, H. In *Molecular Conformation and Dynamics of Macromolecules in Condensed Systems*; Nagasawa, M., Ed.; Elsevier: Amsterdam, The Netherlands, 1988; pp 257−283.

(9) Owens, J. N.; Gancarz, I. S.; Koberstein, J. T.; Russell, T. P. *Macromolecules* **1989**, *22*, 3388.

(10) Winey, K. I.; Thomas, E. L. In *Material Research Society*; Schaefer, D. W., Mark, J. E., Eds.; Elsevier: New York, 1990; Vol. 171, p 255.

(11) Hashimoto, T.; Tanaka, H.; Hasegawa, H. *Macromolecules* **1990**, *23*, 4378.

(12) Tanaka, H.; Hasegawa, H.; Hashimoto, T. *Macromolecules* **1991**, *24*, 240.

(13) Koizumi, S.; Hasegawa, H.; Hashimoto, T. *Makromol. Chem., Macromol. Symp.* **1992**, *62*, 75.

(14) Hashimoto, T.; Koizumi, S.; Hasegawa, H.; Izumitani, T.; Hyde, S. T. *Macromolecules* **1992**, *25*, 1433.

(15) Spontak, R. J.; Smith, S. D.; Ashraf, A. *Macromolecules* **1992**, *25*, 422, 2645.

(16) Hasegawa, H.; Hashimoto, T. In *Comprehensive Polymer Science*, 2nd Suppl.; Aggarwal, S. D., Russo, S., Eds.; Elsevier Science Ltd.: Oxford, 1996; Chapter 14, p 497.

(17) Riess, G.; Schlienger, M.; Marti, S. *J. Macromol. Sci., Polym. Phys. B.* **1980**, *17*, 355.

(18) Arai, K.; Kotaka, T.; Kitano, Y.; Yoshimura, K. *Macromolecules* **1980**, *13*, 1670.

(19) Shibayama, M.; Hasegawa, H.; Hashimoto, T.; Kawai, H. *Macromolecules* **1982**, *5*, 274.

(20) Mogi, Y.; Kotsuji, H.; Kaneko, Y.; Mori, K.; Matsushita, Y.; Noda, I. *Macromolecules* **1992**, *25*, 5408.

(21) Mogi, Y.; Mori, K.; Matsushita, Y.; Noda, I. *Macromolecules* **1992**, *25*, 5412.

(22) Stadler, R.; Auschra, C.; Beckmann, J.; Krappe, U.; Voigt-Martin, I.; Leibler, L. *Macromolecules* **1995**, *28*, 3080.

(23) Krappe, U.; Stadler, R.; Voigt-Martin, I. *Macromolecules* **1995**, *28*, 4558.

(24) Hashimoto, T.; Kimishima, K.; Hasegawa, H. *Macromolecules* **1991**, *24*, 5704.

(25) Hashimoto, T.; Izumitani, T.; Oono, K. *Macromol. Symp.* **1995**, *98*, 925.

(26) Kimishima, K.; Hashimoto, T.; Han, C. D. *Macromolecules* **1995**, *28*, 3842.

(27) Jeon, H. G.; Hudson, S. D.; Ishida, H.; Smith, S. D. *Macromolecules* **1999**, *32*, 1803.

(28) Mango, L. A.; Lenz, R. W. *Die Makromol. Chem.* **1973**, *163*, 13.

(29) Tanaka, Y.; Boochatum, P.; Shimizu, M.; Mita, K. *Polymer* **1993**, *34*, 1098.

(30) Kimishima, K.; Jinnai, H.; Tsutsumi, K.; Hirokawa, Y.; Hashimoto, T., manuscript in preparation.

(31) Hashimoto, T.; Shibayama, M.; Kawai, H. *Macromolecules* **1983**, *16*, 1093.

(32) The difference of electron density between PEP and HPI was much smaller than that between PS and PEP and that between PS and HPI (HPI40 or HPI60). Namely, they are 0.489, 0.503, and 0.567 mol electron/cm^3 for PEP, PI, and PS, respectively. Thus, the scattering contrast for SAXS is effectively that between PS and rubbers, because it is proportional to the square of the difference of electron densities.

(33) Sakurai, S.; Mori, K.; Okawara, A.; Kimishima, K.; Hashimoto, T. *Macromolecules* **1992**, *25*, 2679 and references therein.

(34) ten Brinke, G.; Karasz, R. E.; MackKnight, W. J. *Macromolecules* **1983**, *16*, 1827. Paul, D. R.; Barlow, J. W. *Polymer* **1984**, *25*, 487.
(35) Sakurai, S.; Jinnai, H.; Hasegawa, H.; Hashimoto, T. *Macromolecules* **1991**, *24*, 4839. Sakurai, S.; Izumitani, T.; Hasegawa, H.; Hashimoto, T. *Macromolecules* **1991**, *24*, 4844.
(36) de Gennes, P. G. *J. Phys. (Paris)* **1970**, *31*, 235.
(37) Leibler, L. *Macromolecules* **1980**, *13*, 1602.
(38) Leibler, L.; Benoit, H. *Polymer* **1981**, *22*, 195.
(39) Mori, K.; Tanaka, H.; Hashimoto, T. *Macromolecules* **1987**, *20*, 381.
(40) Ijichi, Y.; Hashimoto, T. *Polym. Commun.* **1988**, *29*, 135.
(41) Kim, J. K.; Kimishima, K.; Hahsimoto, T. *Macromolecules* **1993**, *26*, 125.
(42) Mori, K.; Hasegawa, H.; Hashimoto, T. *Polymer* **1990**, *31*, 2368.
(43) Ehlich, D.; Takenaka, M.; Okamoto, S.; Hashimoto, T. *Macromolecules* **1993**, *26*, 189.
(44) Dalvi, M. C.; Lodge, T. P. *Macromolecules* **1993**, *26*, 859.
(45) Jinnai, H.; Hashimoto, T.; Lee, D.; Chen, S.-H. *Macromolecules* **1997**, *30*, 130. Jinnai, H.; Koga, T.; Nishikawa, Y.; Hashimoto, T.; Hyde, S. T. *Phys. Rev. Lett.* **1997**, *78*, 2248. Hashimoto, T.; Jinnai, H.; Nishikawa, Y.; Koga, T.; Takenaka, M. *Prog. Colloid. Polym. Sci.* **1997**, *106*, 118. Nishikawa, Y.; Jinnai, H.; Koga, T.; Hashimoto, T.; Hyde, S. T. *Langmuir* **1998**, *14*, 1242.
(46) Fetters, L. J.; Lohse, D. J.; Richter, D.; Witten, T. A.; Zirkel, A. *Macromolecules* **1994**, *27*, 4639.

MA981892E